

# Effect of mechanical loading on heterotopic ossification in cervical total disc replacement: a three-dimensional finite element analysis

Danaa Ganbat<sup>1,4</sup> · Yoon Hyuk Kim<sup>1</sup> · Kyungsoo Kim<sup>2</sup> ·  
Yong Jun Jin<sup>3</sup> · Won Man Park<sup>1</sup>

Received: 10 July 2015 / Accepted: 12 December 2015 / Published online: 23 December 2015  
© Springer-Verlag Berlin Heidelberg 2015

**Abstract** The development of heterotopic ossification (HO) is considered one of the major complications following cervical total disc replacement (TDR). Even though previous studies have identified clinical and biomechanical conditions that may stimulate HO, the mechanism of HO formation has not been fully elucidated. The objective of this study is to investigate whether mechanical loading is a biomechanical condition that plays a substantial role to decide the HO formation. A finite element model of TDR on the C5–C6 was developed, and HO formation was predicted by simulating a bone adaptation process under various physiological mechanical loadings. The distributions of strain energy on vertebrae were assessed after HO formation. For the compressive force, most of the HO formation occurred on the vertebral endplates uncovered by the implant footplate which was similar to the Type 1 HO. For the anteriorly directed shear force, the HO was predominantly formed in the anterior parts of both the upper and lower vertebrae as the Type 2 HO. For both the flexion and extension moments, the HO shapes were similar to those for the shear force. The total

strain energy was reduced after HO formation for all loading conditions. Two distinct types of HO were predicted based on mechanically induced bone adaptation processes, and our findings were consistent with those of previous clinical studies. HO formation might have a role in compensating for the non-uniform strain energy distribution which is one of the mechanical parameters related to the bone remodeling after cervical TDR.

**Keywords** Heterotopic ossification · Total disc replacement · Cervical spine · Finite element analysis · Biomechanics

## 1 Introduction

Due to theoretical advantages such as motion preservation, prevention of adjacent segment disease, restoration of intervertebral disc height and segmental lordosis, cervical total disc replacement (TDR) is becoming popular (Alvin et al. 2014; Anderson and Hashimoto 2012; Mummaneni et al. 2007; Phillips and Garfin 2005). Though acceptable and promising clinical outcomes of TDR have been reported, the development of heterotopic ossification (HO) is considered one of the major complications following cervical TDR (Park et al. 2013; Kim and Heo 2013; Leung et al. 2005). In clinical studies, the incidence rate of HO after TDR ranges from 17.8 to 94.1 % (Park et al. 2013; Kim and Heo 2013; Leung et al. 2005). Although spontaneous fusion caused by continuous development of excessive HO around cervical disc arthroplasty has been rarely reported, such outcomes may defeat the main goal of TDR (Parkinson and Sekhon 2005). This contraindication may lead to difficulties when deciding on surgical treatments for patients with disc degeneration.

Danaa Ganbat and Yoon Hyuk Kim have contributed equally to this work as first authors.

✉ Yoon Hyuk Kim  
yoonhkim@khu.ac.kr

<sup>1</sup> Department of Mechanical Engineering, Kyung Hee University, 1 Seocheon-dong, Giheung-gu, Yongin-si, Gyeonggi-do 446-701, Korea

<sup>2</sup> Department of Applied Mathematics, Kyung Hee University, Yongin, Korea

<sup>3</sup> Department of Neurosurgery, Inje University College of Medicine, Seoul Paik Hospital, Seoul, Korea

<sup>4</sup> Present address:  
Department of Technical Mechanics, Mongolian University of Science and Technology, Ulaanbaatar, Mongolia

HO is defined as any bone formation outside the skeletal system and has been reported in the hip, knee, shoulder, elbow, and spinal joints in association with musculoskeletal trauma, spinal cord injury, and central nervous system injury (Pape et al. 2004; Vanden Bossche and Vanderstraeten 2005; Iorio and Healy 2002). However, the etiology of HO is unknown and the clinical assumptions vary (Pape et al. 2004; Vanden Bossche and Vanderstraeten 2005; Iorio and Healy 2002). Even though previous studies have identified clinical and biomechanical conditions that may stimulate HO and it was shown that biomechanical conditions and mechanical loadings were related to HO formation in clinical studies (Park et al. 2013; Kim and Heo 2013; Leung et al. 2005; Suchomel et al. 2010; Yi et al. 2010; Brenke et al. 2012; Jin et al. 2013), the mechanism of HO formation has not been fully elucidated.

Numerous computational simulations of bone remodeling processes have been performed to predict how bone adaptively changes in terms of internal architecture and external shape according to mechanical loading (Huiskes et al. 1987; Weinans et al. 1992; Goel et al. 1995; Grosland and Goel 2007). Several studies have used the bone remodeling algorithms with three-dimensional (3D) finite element (FE) models using the strain energy density (SED) as the mechanical stimuli (Goel et al. 1995; Grosland and Goel 2007). Although two distinct types of HO formation after cervical TDR were simulated with a simple two-dimensional FE model of a single C6 cervical vertebra (Ganbat et al. 2014), no study has yet simulated HO formation using a 3D FE model after cervical TDR. The objective of this study is to investigate the effect of mechanical loading conditions on decision of the shape, location, and amount of HO formation following cervical TDR using a 3D FE model and a common bone remodeling algorithm.

## 2 Materials and methods

### 2.1 A finite element model of a C5–C6 spinal motion segment

A 3D FE model of a human C5–C6 spinal motion segment was constructed from computed tomography (CT) images with the pixel size of 300  $\mu\text{m}$  at 1-mm intervals of slice spacing from a 21-year-old man with a height of 175 cm, based on our previous study (Lee et al. 2011). In order to exclude the additional influences from adjacent segments rather than the loading, a single functional unit consisting of two vertebrae including posterior structures with facet joints, intervertebral disc, and ligaments was modeled. The C5–C6 level was chosen, where TDR is performed most frequently (Suchomel et al. 2010). The cortical bone and vertebral endplate are both modeled with 0.5 mm of thicknesses. The

facet joint is modeled with cartilage which has 0.5 mm of thickness and 0.25 mm of joint space between the articular surfaces. The intervertebral disc was modeled with the annulus surrounding circumferentially the nucleus pulposus at the center, where the annulus had five-layered ground substance surrounded by six-layered annulus fibrosus (Lee et al. 2011). The annulus fibrosus with the 3D tension-only truss elements was positioned a mean of  $25^\circ$  against the horizontal plane, and its cross-sectional area was set up to account for 20% of the volume of the annulus. The anterior longitudinal ligament, posterior longitudinal ligament, interspinous ligament, supraspinous ligament, capsular ligament, and flaval ligament were modeled with the 3D tension-only truss elements (Fig. 1a). The material properties were obtained from the literature (Lee et al. 2011) (Table 1). For validation, RoMs of the intact FE model were compared to those in a previous experimental study (Moroney et al. 1988) under the flexion, extension, lateral bending, and axial torsion of 1.8 Nm with a compression force of 73.6 N.

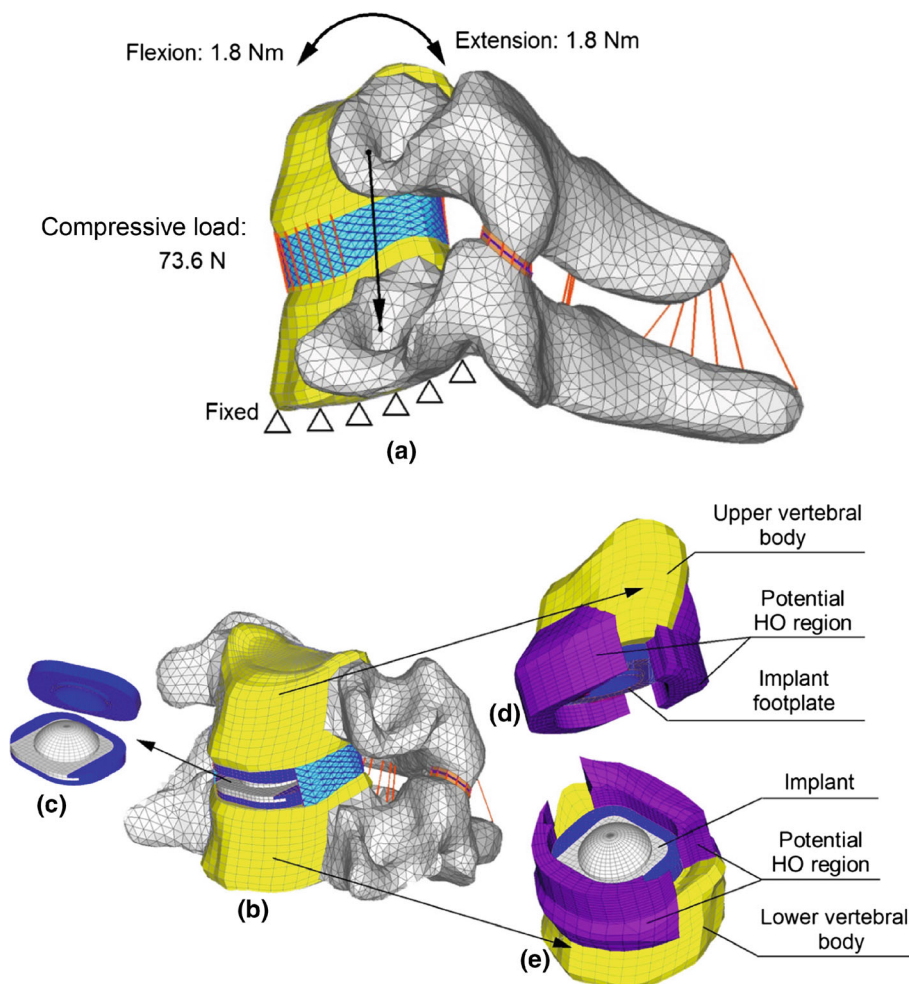
### 2.2 A finite element model of TDR on C5–C6

A 3D FE model of a Prodisc-C (Synthes Inc., West Chester, PA, USA) artificial disc was developed based on a reverse engineering from the technical guide document (Synthes Inc 2007) (Fig. 1c). The dimension used in this study was decided based on the Implant L from the document with an article number of SSC306C, including a radius of spherical part. The overall dimension of the Prodisc-C was 17 mm  $\times$  14 mm  $\times$  6 mm, and the radius of spherical part was 5.5 mm. The Prodisc-C consisted of cobalt chrome alloy upper and lower footplates and an ultra-high molecular weight polyethylene core, where the material properties were obtained from a previous study (Lee et al. 2011) (Table 1). The core was fixed to the lower footplate, and the friction coefficient between the upper implant footplate and the core was assumed to be 0.07 (Lee et al. 2011). A FE model of TDR on the C5–C6 was then created from an intact FE model by inserting Prodisc-C based on the standard surgical protocol (Rohmann et al. 2005; Galbusera et al. 2008) (Fig. 1b).

### 2.3 Potential HO regions

To predict HO formation, potential HO regions were initially predefined at the anterior and posterior edges of the vertebrae of the implanted FE model (Fig. 1d, e). The initial location of the potential HO regions was chosen based on clinical observations of HO formation (Yi et al. 2012; Jin et al. 2013), which reported that HO was mostly created at the anterior and posterior edges of the implanted vertebrae. Its initial size was determined based on analyses of clinical X-ray images (Yi et al. 2012; Jin et al. 2013). A preliminary analysis showed that the initial size was large

**Fig. 1** Developed three-dimensional finite element (FE) models. **a** FE model of C5–C6 with loading and boundary conditions for validation; **b** FE model of TDR on C5–C6; **c** FE model of Prodisc-C; **d** upper vertebral body with potential HO region; **e** lower vertebral body with potential HO region



enough not to affect the convergence results. A sensitive analysis was also conducted with different initial densities for potential HO regions in order to decide the initial density of the potential HO regions. The initial density  $\rho$  for the HO regions was then assumed to be  $0.73 \text{ g/cm}^3$ , which was half of the cortical bone density as the previous bone remodeling studies (Weinans et al. 1992; Goel et al. 1995; Grosland and Goel 2007), where the cortical bone density of  $1.47 \text{ g/cm}^3$  was calculated from its Young’s modulus of  $12000 \text{ MPa}$  assumed in this study and the relationship  $E = 3790\rho^3$  (Carter and Hayes 1977; Weinans et al. 1992). The Young’s modulus of  $1474 \text{ MPa}$  for the HO regions was then obtained by applying the initial density of  $0.73 \text{ g/cm}^3$  to the relationship. Poisson’s ratio was set to  $0.29$  for cortical and cancellous bones (Weinans et al. 1992; Lee et al. 2011).

### 2.4 Bone remodeling algorithm

The SED was chosen as the local stimulus for the bone remodeling algorithm (Huiskes et al. 1987; Weinans et al.

1992; Goel et al. 1995; Grosland and Goel 2007) and calculated using ANSYS<sup>®</sup> (ANSYS, Inc., Canonsburg, PA, USA). The iteration procedure is executed by MATLAB<sup>®</sup> (The MathWorks Inc., Natick, MA, USA). The bone density  $\rho$  at each element in the potential HO region was then modified by the SED value  $S$  and the homeostatic SED value  $K$  as follows (Weinans et al. 1992; Huiskes et al. 1987):

$$\frac{d\rho}{dt} = \begin{cases} B_r (S - K (1 + s)), & S \geq K (1 + s) \\ 0, & K (1 - s) \leq S \leq K (1 + s) \\ B_f (S - K (1 - s)), & S \leq K (1 - s) \end{cases}$$

where  $B_r$  and  $B_f$  are the remodeling rate coefficients for resorption and formation, respectively, and  $s$  is the threshold level of the lazy zone (Carter and Hayes 1977). The lazy zone is a range of SED where the bone density is not changed under a loading condition. In the bone remodeling algorithm, the lazy zone was defined as  $K (1 - s) \leq S \leq K (1 + s)$  with the homeostatic SED value  $K$  and the threshold level  $s$ . The values of the bone remodeling parameters were taken from a preliminary analysis based on previous studies (Huiskes et al. 1987; Weinans et al. 1992; Ganbat

**Table 1** Material properties used in the finite element (FE) model, adopted from the literature (Lee et al. 2011)

	Young's modulus (MPa)	Poisson's ratio	Cross-sectional area (mm <sup>2</sup> )
<i>Vertebra</i>			
Cortical bone	12,000	0.29	–
Cancellous bone	450	0.29	–
Posterior bone	3500	0.29	–
Vertebral endplate	500	0.4	–
Facet cartilage	10.4	0.4	–
<i>Disc</i>			
Nucleous	1	0.49	–
Annulus ground substance	3.4	0.4	–
Annulus fibrosus	110	0.3	–
<i>Ligaments</i>			
Anterior longitudinal	10	0.3	6.0
Posterior longitudinal	10	0.3	5.0
Capsular	10	0.3	46.0
Flaval	1.5	0.3	5.0
Interspinous	1.5	0.3	10.0
Supraspinous	1.5	0.3	5.0
<i>Artificial disc</i>			
CoCr alloy for implant footplate	210,000	0.3	–
Ultra-high molecular weight polyethylene for implant core	3000	0.3	–

et al. 2014): homeostatic SED value  $K = 0.00025$  J/g, threshold level of the lazy zone  $s = 0.2$ , time unit is chosen for days of month  $\Delta t = 30$ , the remodeling rate coefficient  $B = 1.0$  (g/cm<sup>3</sup>)<sup>2</sup>/(MPa × time unit), and  $B_r = B_f = B \Delta t$ . In order to mimic cyclic loading conditions, the homeostatic SED value of  $K = 0.00025$  J/g was chosen. The bone density modification was iteratively repeated until the difference in the total strain energy at the present step from that at the previous step in the FE model was less than  $10^{-11}$  J. When the iterative process was finished, elements with bone density of zero were removed from the potential HO regions. The amount of HO formation with respect to the region and changes in strain energy after HO formation were investigated. The HO formations were simulated at each vertebra separately without considering any connection of HO formations at the lower and the upper vertebrae, such as fusion and bridging, to focus on the loading conditions.

## 2.5 Loading conditions

In order to study the effects of loading conditions on HO formations, bone adaptation simulations were performed for (a)

a compressive force of 100 N; (b) anteriorly directed shear force of 100 N; (c) a flexion of 1.5 Nm; (d) an extension of 1.5 Nm; (e) a flexion of 1.5 Nm with a compression of 100 N; and (f) an extension of 1.5 Nm with compression of 100 N. The compressive force of 100 N was chosen based on the literature (Galbusera et al. 2008). The compressive force was applied from the upper vertebral center to the lower vertebral center as the follower load. The magnitude of the shear force was decided to be the same as the compressive force in order to compare the effect of loading conditions (Ganbat et al. 2014). The shear force was applied at the upper vertebral center to the direction parallel to the upper implant footplate. In order to mimic more realistic loading conditions to create shear forces which are experienced in daily activities, the flexion and extension moments of 1.5 Nm were chosen with and without a compressive force of 100 N based on the literature (Moroney et al. 1988; Rohlmann et al. 2005; Galbusera et al. 2008; He and Xinghua 2006). The flexion and extension moments were applied at the upper vertebral center.

## 3 Results

The RoM of intact FE model of the C5–C6 for flexion–extension was 8.4°, while it was 5.3°–12.9° in a previous experimental study (Moroney et al. 1988). In lateral bending and axial rotation, the RoMs of the intact FE model were 1.7° and 2.2°, respectively, while they were 1.7°–7.7° and 1.2°–2.5°, respectively, in the previous experimental study (Moroney et al. 1988).

For the compressive force of 100 N, most of the HO formation occurred on the vertebral endplates uncovered by the implant footplate which was similar to the Type 1 HO (Jin et al. 2013) (Fig. 2a; Table 2a). For the anteriorly directed shear force of 100 N, the HO was predominantly formed in the anterior parts of both the upper and lower vertebrae as the Type 2 HO (Jin et al. 2013) (Fig. 2b; Table 2b). For both the flexion and extension moments of 1.5 Nm, the HO shapes were similar to those for the shear force (Table 2c, d). For the flexion of 1.5 Nm with the compression of 100 N, the HO formation occurred mainly in anterior parts of vertebrae and was originated from the mid-level of the cortical shell as the Type 2 HO (Table 2e). For the extension of 1.5 Nm with the compression of 100 N, the HO formation dominantly occurred in the posterior parts, where the anterior part of the upper vertebra had HO formation mainly from the cortical shell. In the lower vertebra, the HO formation shape was a combination of both Type 1 and Type 2 HO (Table 2f).

The total strain energy was reduced after HO formation for all loading conditions (Table 3). Moreover, the peak value of the strain energy in the anterior region of the upper vertebra near the implant footplate was reduced from 4.56 to 2.44 μJ, while it decreased from 3.42 to 2.75 μJ in the lower verte-



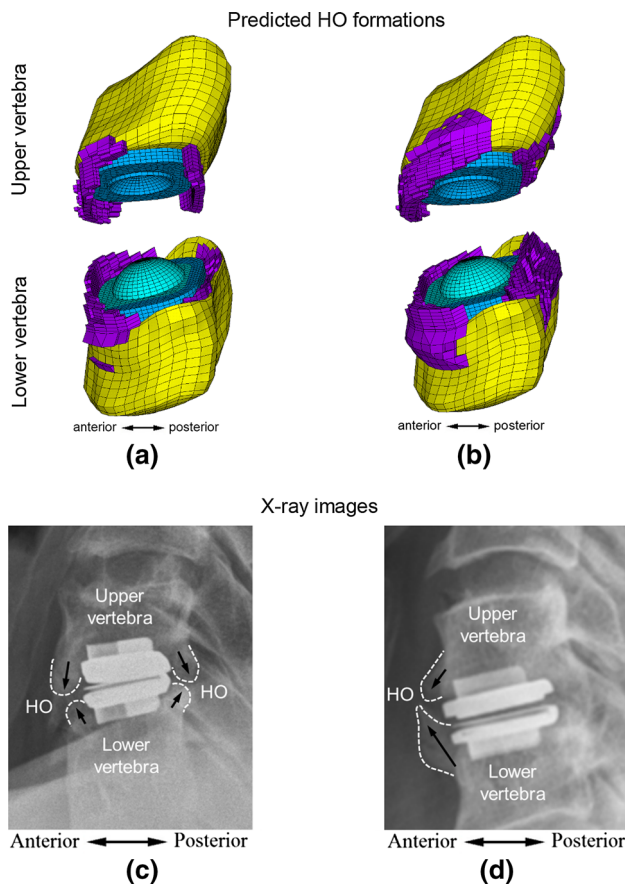


**Fig. 2** Comparison between predicted HO formations for compressive and shear forces and X-ray images for the Type 1 and Type 2 HO. **a** Compressive force of 100 N; **b** Anterior shear force of 100 N. **c** Type 1 HO; **d** Type 2 HO

bra for the flexion with the compression (Fig. 3a). For the extension with the compression, the peak value of the strain energy in the posterior region of the upper vertebra near the implant footplate was reduced from 14.14 to 6.05  $\mu\text{J}$ , while it decreased from 7.92 to 5.58  $\mu\text{J}$  in the lower vertebra (Fig. 3b).

#### 4 Discussion

The shapes of HO for the compressive and shear forces were consistent with those observed in clinical settings in terms of the origin and growing direction of HO formation (Fig. 2). The HO formation for the compressive force of 100 N was similar to the Type 1 HO (Jin et al. 2013), which was defined as a bone mass that protruded from the residual vertebral endplate uncovered by implant footplates of the prosthesis or vertebral body edges, and was grown in the outside directions (Fig. 2c). For the anteriorly directed shear force, the HO formation was similar to the Type 2 HO (Jin et al. 2013), where the Type 2 HO is originated from the mid-body level of the vertebral body rather than the vertebral endplate and

grows in the superior direction in the lower vertebra or the inferior direction in the upper vertebra (Fig. 2d). In addition, the HO formations for the flexion and extension (Table 2d, e) were similar with those created under directed shear forces (Table 2b). The shear displacements were possibly created under flexion and extension in the cervical segment (Moroney et al. 1988). The flexion and extension were regarded to create the Type 2 HO as the shear force.

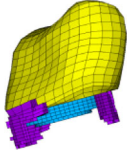
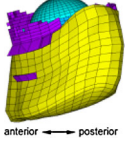
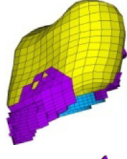
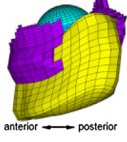
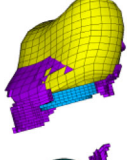
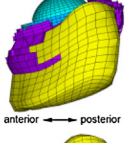
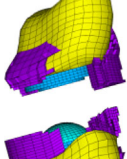
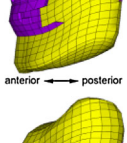
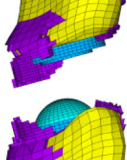
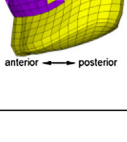
In daily activities, human cervical spine experiences not only pure flexion and extension but also the compression from head weight. Thus, simulations to predict HO formations for the flexion and extension with the compression were performed. The addition of the compressive force to the flexion increased HO formation in volume at the anterior parts of the upper and lower vertebrae by 11.4 and 48.2%, respectively, while HO at the posterior parts of the upper and lower vertebrae decreased by 51.5 and 54.9%, respectively (Table 2c, e). A similar phenomenon was also observed for the extension with the compression: The HO formation at the posterior part of the upper and lower vertebrae increased by 12.3 and 32.7%, respectively, while HO volume decreased by 25.4 and 6.8% at the anterior parts of the upper and lower vertebrae, respectively (Table 2d, f). Therefore, the compression influenced the HO formation on anterior and posterior regions of vertebrae differently depending on applied flexion or extension which is combined with compression.

HO formation itself subsequently decreased the peak values and total values of the strain energy, regardless of the applied loading conditions (Fig. 3; Table 3). Thus, HO formation might play a role in compensating for the non-uniform strain energy distribution following cervical TDR. Since the strain energy is one of the mechanical parameters related to the bone fracture (Huiskes et al. 1987; Goel et al. 1995), this result indicates that HO might be originated to reduce the possibility of fracture.

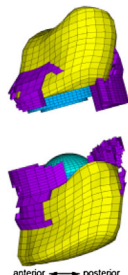
The reduction of strain energy was greater in the upper vertebra than lower vertebra for both the flexion and extension. These results support the data reported that the occurrence of HO in the antero-inferior disc and postero-inferior disc space is much lower than that in the antero-superior and postero-superior disc spaces (Jin et al. 2013). In addition, the reduction in strain energy was greater in the posterior region, which was not covered by the implant footplate for the extension with compression. Since an implant may not cover the whole vertebral endplate due to surgical restrictions, our results support the hypothesis that the occurrence of HO may be reduced when the area of the implant footplate on the vertebral endplate is increased from the mechanical point of view.

According to the above result, we hypothesized about the details of HO formation. From the biological point of view, a bony microenvironment is likely to stabilize through the bone remodeling process. Non-uniform SED seems to be

**Table 2** Volume and shape of heterotopic ossification (HO) formation for parts of the vertebral bodies (unit: mm<sup>3</sup>)

Loading conditions	Vertebral body	Anterior part of vertebra	Posterior part of vertebra	Predicted HO formation shapes
(a) Compression of 100 N	Upper vertebra	120.77	86.72	
	Lower vertebra	126.53	36.64	
(b) Anteriorly directed shear force of 100 N	Upper vertebra	203.97	31.00	
	Lower vertebra	330.09	214.68	
(c) Flexion of 1.5 Nm	Upper vertebra	290.69	50.40	
	Lower vertebra	139.21	175.74	
(d) Extension of 1.5 Nm	Upper vertebra	160.58	394.38	
	Lower vertebra	364.81	204.50	
(e) Flexion of 1.5 Nm with compression of 100 N	Upper vertebra	323.91	24.45	
	Lower vertebra	206.27	79.09	

**Table 2** continued

Loading conditions		Vertebral body	Anterior part of vertebra	Posterior part of vertebra	Predicted HO formation shapes
(f)	Extension of 1.5 Nm with compression of 100 N	Upper vertebra	119.78	442.71	
		Lower vertebra	340.03	303.90	

**Table 3** Reduction in total strain energy in vertebrae after heterotopic ossification (HO) formation (unit:  $\mu\text{J}$ )

Loading condition		Before HO	After HO	Decreased %
(a)	Compression of 100 N	619.8	609.1	1.7
(b)	Anteriorly directed shear force of 100 N	2965.8	2606.8	12.1
(c)	Flexion of 1.5 Nm	2369.4	2176.2	8.2
(d)	Extension of 1.5 Nm	3801.9	3089.5	18.7
(e)	Flexion of 1.5 Nm with compression of 100 N	2896.7	2630.4	9.2
(f)	Extension of 1.5 Nm with compression of 100 N	4596.6	3629.4	21.0

related to microdamage occurring in the cortical and cancellous bone around the footplates. Microdamage-induced osteocyte apoptosis activates the coupled action of osteoclasts and osteoblasts and facilitates bone resorption and formation. Remodeling usually stops without stimuli by compression. However, the stimuli may be unstoppable in the mobile instrumented disc space. This maladaptive process is expected to continue until stimuli like SED diminish to some degree. If HO formation follows this well-known remodeling process, it may grow larger. However, the growth of HO decreases SED and increases the stability around footplate so that HO may not grow. In clinical settings, this process is similar to the formation of degenerative osteophytes for spinal stability. Therefore, HO may be considered as a kind of osteophyte.

Validation of the current intact model was conducted by comparing the RoM with previous experimental data (Moroney et al. 1988). All RoMs of the current intact FE model of the C5–C6 were within the range of results reported in the previous experimental study even though the RoMs in lateral bending and axial rotation were near the boundaries of experimental results (Moroney et al. 1988). Since this study mainly dealt with the flexion and extension, these results confirmed the validity of our FE model of the C5–C6.

There are several limitations and restrictions to this study. Due to several technical difficulties, such as long computation time with huge number of elements in the 3D FE model, we simplified the simulation as to predict the shape, location, and amount of HO influenced by mechanical loading

conditions. In addition, the bone formation was allowed only within the elements of HO regions. Although we did not simulate HO formation by the direct step by step way as in (He and Xinghua 2006), the resultant HO formations were clearly distinguished for different loadings. Connection of HO formations between the lower and upper vertebrae, which can affect the mechanical loading conditions, was not considered in this study. The linear elastic material properties for the FE model were used in this study based on a previous study (Lee et al. 2011). The realistic nonlinear, hyper-elastic, or multiphase models can enhance the accuracy and confidence of simulation results because the SED values are dependent on the material properties. Parameters related to the bone remodeling algorithm, such as the homeostatic SED and the threshold level of the lazy zone, were derived primarily from studies on the femur or decided artificially based on a preliminary analysis, due to the lack of relevant physiological data for vertebral bone, particularly cervical bone. An initial density for the HO region was predefined as an entirely artificial initial condition, while the stiffness assigned to these regions is important in deriving the SED in the elements. Hence, the sensitivity analysis of parameters related to the bone remodeling algorithm and the initial conditions is necessary to improve the relevance of bone remodeling results. Since various alignments of the cervical spine can affect on the direction and magnitude of loading, 3D FE models of the whole cervical spine from several subjects can enhance the relevance of this study. Complicated loadings in daily activities with consideration of muscle forces may also be

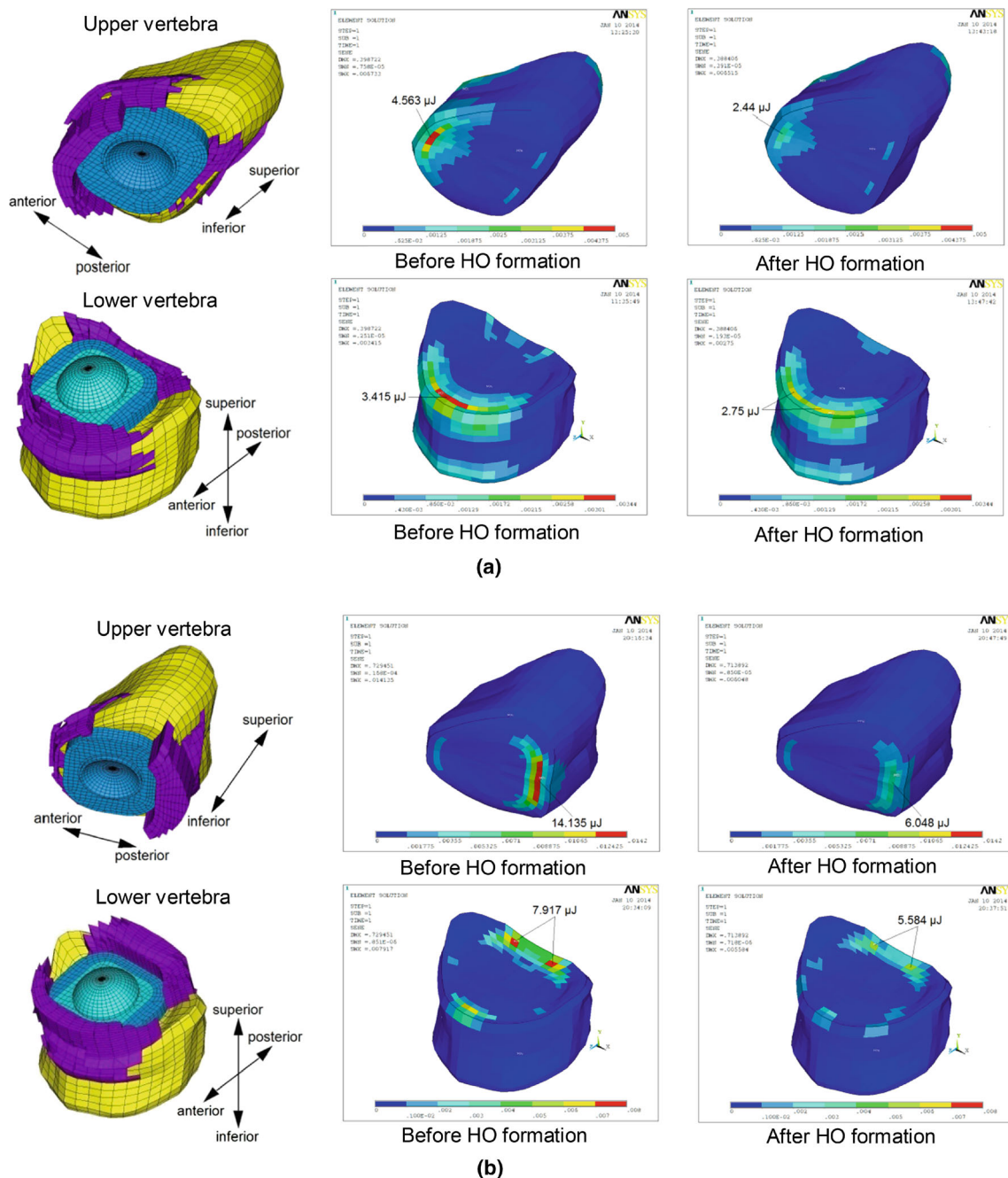


**Fig. 3** Strain energy distribution in vertebrae before and after HO formation. The peak values of strain energy were reduced after HO formation. **a** Flexion of 1.5 Nm with compression of 100 N. **b** Extension of 1.5 Nm with compression of 100 N

necessary. In addition, bone adaptation theories incorporating stress, strain, and SED can also contribute to realistic predictions of HO.

In conclusion, two distinct types of HO following cervical TDR were predicted based on mechanically induced bone adaptation processes, and our findings were consistent with those of previous clinical studies. The predicted HO formation shapes could be considered as the same shape as real HO visible on X-ray images under physiological loading condi-

tions. HO formation might have a role in compensating the non-uniform strain energy distribution which is one of the mechanical parameters related to bone fracture. The uniform distribution of strain energy on vertebrae after HO formation suggests that the growth would stop by means of bone remodeling of segmental stabilization by degenerative osteophytes. It is meaningful that we present the effects of different mechanical loading conditions on HO occurrence following cervical TDR for the first time using a 3D FE model.



Finally, our results may be applicable to the design of artificial discs that minimize HO. In the future, it is clinically challenged to investigate what loading conditions or scenarios do not develop the HO by considering various factors, such as dimensions of the vertebra and artificial disc, coverage area by the footplate, and location of the artificial disc on the vertebra.

**Acknowledgments** This work was supported by the National Research Foundation of Korea (NRF) grant funded by the Korea government (Ministry of Science, ICT and Future Planning) (NRF-2014K2A4A1034553).

#### Compliance with ethical standards

**Conflict of interest** All authors declare that they have no conflict of interest.

## References

- Alvin MD, Abbott EE, Lubelski D, Kuhns B, Nowacki AS, Steinmetz MP, Benzel EC, Mroz TE (2014) Cervical arthroplasty: a critical review of the literature. *Spine J* 14(9):2231–2245
- Anderson PA, Hashimoto R (2012) Total disc replacement in the cervical spine: a systematic review evaluating long-term safety. *Evid Based Spine Care J* 3(S1):9–18
- Brenke C, Scharf J, Schmieder K, Barth M (2012) High prevalence of heterotopic ossification after cervical disc arthroplasty: outcome and intraoperative findings following explantation of 22 cervical disc prostheses. *J Neurosurg Spine* 17(2):141–146
- Carter DR, Hayes WC (1977) The compressive behavior of bone as a two-phase porous structure. *J Bone Joint Surg Am* 59(7):954–962
- Galbusera F, Bellini CM, Raimondi MT, Fornari M, Assietti R (2008) Cervical spine biomechanics following implantation of disc prosthesis. *Med Eng Phys* 30(9):1127–1133
- Ganbat D, Kim K, Jin YJ, Kim YH (2014) Heterotopic ossification in cervical total disc replacement: a finite element analysis. *Proc Inst Mech Eng H* 228(2):200–205
- Goel VK, Ramirez SA, Kong W, Gilbertson LG (1995) Cancellous bone Young's modulus variation within the vertebral body of a ligamentous lumbar spine-application of bone adaptive remodeling concepts. *J Biomech Eng* 117(3):266–271
- Grosland NM, Goel VK (2007) Vertebral endplate morphology follows bone remodeling principles. *Spine* 32(23):E667–673
- He G, Xinghua Z (2006) The numerical simulation of osteophyte formation on the edge of the vertebral body using quantitative bone remodeling theory. *Joint Bone Spine* 73(1):95–101
- Huiskes R, Weinans H, Grootenboer HJ, Dalstra M, Fudala B, Slooff TJ (1987) Adaptive bone-remodeling theory applied to prosthetic-design analysis. *J Biomech* 20(11–12):1135–1150
- Iorio R, Healy WL (2002) Heterotopic ossification after hip and knee arthroplasty: risk factors, prevention, and treatment. *J Am Acad Orthop Surg* 10(6):409–416
- Jin YJ, Park SB, Kim MJ, Kim KJ, Kim HJ (2013) An analysis of heterotopic ossification in cervical disc arthroplasty: a novel morphologic classification of an ossified mass. *Spine J* 13(4):408–420
- Kim KS, Heo DH (2013) Do postoperative biomechanical changes induce heterotopic ossification after cervical arthroplasty? A 5-year follow-up study. *J Spinal Disord Tech*. doi:10.1097/BSD.000000000000054
- Lee SH, Im YJ, Kim KT, Kim YH, Park WM, Kim K (2011) Comparison of cervical spine biomechanics after fixed- and mobile-core artificial disc replacement: a finite element analysis. *Spine* 36(9):700–708
- Leung C, Casey AT, Goffin J, Kehr P, Liebig K, Lind B, Logroscino C, Pointillart V (2005) Clinical significance of heterotopic ossification in cervical disc replacement: a prospective multicenter clinical trial. *Neurosurgery* 57(4):759–763
- Moroney SP, Schultz AB, Miller JA, Anderson GB (1988) Load-displacement properties of lower cervical spine motion segments. *J Biomech* 21(9):769–779
- Mummaneni PV, Burkus JK, Haid RW, Traynelis VC, Zdeblick TA (2007) Clinical and radiographic analysis of cervical disc arthroplasty compared with allograft fusion: a randomized controlled clinical trial. *J Neurosurg Spine* 6(3):198–209
- Pape HC, Marsh S, Morley JR, Krettek C, Giannoudis PV (2004) Current concepts in the development of heterotopic ossification. *J Bone Joint Surg Br* 86(6):783–787
- Park JH, Rhim SC, Roh SW (2013) Mid-term follow-up of clinical and radiologic outcomes in cervical total disc replacement (Mobi-C): incidence of heterotopic ossification and risk factors. *J Spinal Disord Tech* 26(3):141–145
- Parkinson JF, Sekhon LH (2005) Cervical arthroplasty complicated by delayed spontaneous fusion. Case report. *J Neurosurg Spine* 2(3):377–380
- Phillips FM, Garfin SR (2005) Cervical disc replacement. *Spine* 30(17 Suppl):S27–S33
- Rohmann A, Zander T, Bergmann G (2005) Effect of total disc replacement with Prodisc on intersegmental rotation of the lumbar spine. *Spine* 30(7):738–743
- Suchomel P, Jurák L, Benes V III, Brabec R, Bradác O, Elgawhary S (2010) Clinical results and development of heterotopic ossification in total cervical disc replacement during a 4-year follow-up. *Eur Spine J* 19(2):307–315
- Synthes Inc (2007) Technique guide: Prodisc-C. Modular intervertebral disc prosthesis for restoring disc height and segmental motion in the cervical spine. Synthes, Inc. <http://sites.synthes.com/MediaBin/International%20DATA/036.000.431.pdf>
- Vanden Bossche L, Vanderstraeten G (2005) Heterotopic ossification: a review. *J Rehabil Med* 37(3):129–136
- Weinans H, Huiskies R, Grootenboer HJ (1992) The behavior of adaptive bone-remodeling simulation models. *J Biomech* 25(12):1425–1441
- Yi S, Kim KN, Yang MS, Yang JW, Kim H, Ha Y, Yoon DH, Shin HC (2010) Difference in occurrence of heterotopic ossification according to prosthesis type in the cervical artificial disc replacement. *Spine* 35(16):1556–1561